Perovskites Solar Cells



www.advmatinterfaces.de

Intrinsic Behavior of CH₃NH₃PbBr₃ Single Crystals under Light Illumination

Benjamin R. Ecker, Congcong Wang, Haotong Wei, Yongbo Yuan, Jinsong Huang, and Yongli Gao*

Single crystal CH3NH3PbBr3 samples are exposed to light illumination, with a light intensity about seven times stronger than the sun while under ultrahigh vacuum (UHV) conditions, in order to investigate their chemical and structural stability from prolonged light illumination. X-ray photoemission spectroscopy measurements show that within 10 h of illumination, about half of the initial C, N, and Br elemental concentrations leave the surface and about half of the perovskite's Pb is converted into metallic Pb. Light exposures while in the UHV system also significantly roughen the surface, and surprisingly, empty voids form ≈1 to 3 µm down in the light exposed region. A framework based on the Kirkendall effect is put forward to explain the observed void formation. This proposed model may be relevant to the slow degradation of perovskite solar cells, which is sometimes attributed to irreversible chemical reactions from undesired diffusion. These measurements and observations reveal the intrinsic behavior of the CH3NH3PbBr3 single crystals under light illumination while in a UHV system where volatile species are free to leave, in contrast to existing device studies on the photostability of perovskite solar cells.

1. Introduction

Since their first use in a dye-sensitized solar cell back in 2009 by Miyasaka and co-workers, [1] hybrid organic inorganic perovskites (HOIPs) have been the focus of considerable and intense research efforts due to their potential use in a next generational solar cell. This fierce research effort by the community has led

B. R. Ecker, Dr. C. Wang, Prof. Y. Gao Department of Physics and Astronomy University of Rochester Rochester, NY 14627, USA E-mail: ygao@pas.rochester.edu Dr. H. Wei, Prof. J. Huang Department of Applied Physical Sciences

University of North Carolina

Chapel Hill, NC 27599, USA

Prof. Y. Yuan

School of Physics and Electronics

Hunan Key Laboratory of Super Microstructure and Ultrafast Process Central South University

Changsha, Hunan 410083, China

(D)

The ORCID identification number(s) for the author(s) of this article can be found under https://doi.org/10.1002/admi.201801206.

DOI: 10.1002/admi.201801206

to impressive improvement to the device's power conversion efficiency (PCE), with the most recent highest certified report at 23.3% in 2018.[2] While there has been rapid growth in the PCE of the HOIPbased solar cells, they still face numerous challenges to their ultimate long term operational use including the ecotoxicity of the device materials over their lifecycle, [3] various operational phenomena that appear to deteriorate device performance such as hysteresis^[4] and ion migration,^[5] and perhaps the most concerning matter, their degradation due to various environmental exposures. The most well documented perovskite device degradation pathway has been attributed to moisture exposure, and indeed we have previously seen that CH₃NH₃PbI₃ and CH₃NH₃PbBr₃ perovskites are sensitive to moisture and begin to decompose at a certain threshold of water exposure. [6,7] External heating has also been suggested as a potential stability

issue, and substantial heating has been shown to seriously deteriorate device performances as the various layers, including the perovskite layer, decompose.^[8,9] Reasonably small applied voltages have also been seen to directly induce poling and ion migration, and ionic migration has widely been discussed as a main contribution to the observed hysteresis phenomena.^[10,11] Another potential degradation pathway that has not received enough attention and discussion is the possible influence of light illumination on the HOIP layer. Indeed, the perovskite layer makes up the very heart of the solar cell device and it is ultimately responsible for the generation of charge carriers. It is therefore imperative to understand the stability of the perovskite layer under solar irradiation.

Early on in 2013, Snaith and co-workers attributed the illumination induced degradation of perovskite solar cells to the ultraviolet light induced desorption of oxygen from the mesoporous ${\rm TiO_2}$ used as the hole transport layer in their devices, they then further suggested ${\rm Al_2O_3}$ as an alternative. Then later in 2015, Murugadoss et al. further confirmed that various perovskite films under visible and ultraviolet illumination were indeed more stable on ${\rm Al_2O_3}$ compared with ${\rm TiO_2}$. While the ${\rm TiO_2}$ hole transport layer is still widely used despite this instability issue, more recent high performance devices are opting for alternative materials such as La doped ${\rm BaSnO_3}$. The influence of light on the degradation of HOIP material in various



gas environments including ambient air was shown by Bryant et al. in early 2016.^[15] Near the same time, two slightly conflicting reports came out by Yuan et al.^[16] and Merdasa et al.^[17] While both reports showed strong material degradation under illumination, the first report saw very little photoluminescent (PL) spectral shifts, but the second report saw a continuous blue PL spectral shift. The differences in the observed spectral shifts could most likely be attributed to the amount of light fluence and the bulk versus surface decompositions seen in the two cases.

Very recently, we presented our surface analytic study on the degradation of coevaporated CH2NH3PbI3 thin films by light exposure, which provided evidence that perovskite degradation by light is limited and restricted by the diffusion process to the surface.^[18] This would certainly suggest that the discrepancy observed in refs. [16] and [17] was at least partially due to the difference in sample geometry and surface area. It also demonstrated that important insight may be obtained with surface analytical probes. Though, sample preparation that is compatible with surface analysis is not easily obtained for perovskite materials, especially with the common spin coat film formation techniques.^[19] Other investigations into mixed halide perovskites samples with compositions similar to those used in high performance devices have also reported photoinduced changes. A surface analytical investigation^[20] revealed distinctly different photobleaching behavior between mixed halide spin coated CH₃NH₃PbI_{3-x}Cl_x and CH₃NH₃PbBr_{3-x}Cl_x films, where no metallic Pb was produced in their mixed Br/Cl halide film study. This result remains strikingly different than their mixed I/Cl halide film, our previous I thin film investigation, and the following report on a purely Br halide single crystal. Meanwhile, optical and structural investigations [21,22] on mixed halide thin films and single crystals, which are more sensitive to the bulk of the sample than the surface, suggested reversible photoinduced physical and electronic structural changes including segregation into Br and I rich regions. The numerous photoinduced reports beg further investigations of the perovskite films and full devices for a more complete understanding of the underlying physics and chemistry that is occurring under illumination and potential impacts on device applications.

Here we present our investigation on the stability of CH3NH3PbBr3 single crystals under light illumination in an ultrahigh vacuum (UHV) system. Due to their large mobilities and carrier lifetimes, the HOIP single crystals have been suggested to have applications as photodetectors or the active laser material. In particular, the CH₃NH₃PbBr₃ single crystals have previously been shown to be a highly efficient X-ray detector. [23] Pristine fresh surfaces of the high quality crystals were created by cleaving the top layer off in the UHV system, which was primarily used to eliminate other possible environmental factors. A blue continuous wave (CW) semiconductor laser with a wavelength of 408 nm and intensity about seven times the AM 1.5 standard irradiation (≈1000 W m⁻²) was used to illuminate a region of the crystal for fixed timed periods, and X-ray photoemission spectroscopy (XPS) measurements were then made immediately after each timed exposure. Strong chemical degradation was observed after the light exposures in the UHV system, and a new spectral component appeared in the Pb core level spectra and was attributed to metallic Pb. The crystal's

surface changed from a translucent orange to a dull metallic silver after the full exposure of 44 h, and these surface morphological changes were investigated with a scanning electron microscope (SEM) and with microscopic trenches milled by a focused ion beam (FIB). The FIB milled trenches revealed that large voids had formed 1-3 µm down into the material in the light exposed region. A thin vertical slice, or lamella, was removed from the sample by an FIB liftout process in order to investigate these structural changes with a transmission electron microscope (TEM). The TEM images, energy dispersive X-ray spectroscopy characterizations, and electron diffraction patterns further confirmed the chemical and morphological changes seen by the XPS measurements and SEM images. These combined observations strongly suggest that the light illumination in the UHV system induced substantial material and structural degradation, and a purely diffusion based model is then proposed to explain the void formation. The model is contextualized with relevant HOIP diffusion and ion migration discussions, and the phenomena's potential wider implications are briefly discussed. These experiments revealed the intrinsic behavior of the CH3NH3PbBr3 single crystals under light illumination while in a UHV system where the degraded volatile components could readily leave the surface. By contrast, a real HOIP device's structure and packaging may inhibit the degraded components from leaving the perovskite layer.

2. XPS Results and Discussions

The high quality CH₂NH₃PbBr₃ single crystals used in the following investigations were grown by the antisolvent method and have previously been studied by powder X-ray diffraction,[23,24] but they were additionally characterized here with a textured X-ray diffraction (XRD) study. The results revealed that the samples were indeed (100) oriented crystals with the (110) plane at 45° to the surface plane, and they further confirmed that the crystals had a cubic structure with an associated lattice constant of 5.92 Å. The samples were prepared and mounted in such a way that the top surface could be cleaved off in the UHV system (in situ), and this cleaving created a pristine surface necessary for reliable photoemission spectroscopy studies. The freshly cleaved surface was initially measured by XPS, and then it was exposed to light for a fixed amount of time, before repeating the measurements and exposures contiguously. The light source used for exposure was a small semiconductor diode laser with a wavelength of 408 nm and an intensity about seven times the standard AM1.5 solar irradiance. The higher illumination intensity was selected to ascertain that effects due to light exposure, as any light induced effects were initially thought to be quite small as some devices have remained stable for 1000 to 10 000 of hours of continuous illumination. Additional information regarding the samples and the measurement processes are described in the Experimental Section, and the XRD results are displayed in Figures S1 and S2 of the Supporting Information.

A striking visible change in the crystal's surface was observed in the microscope during the measurement process, but was fully revealed when the sample was removed. In the region that was exposed to the illumination, the crystal surface changed

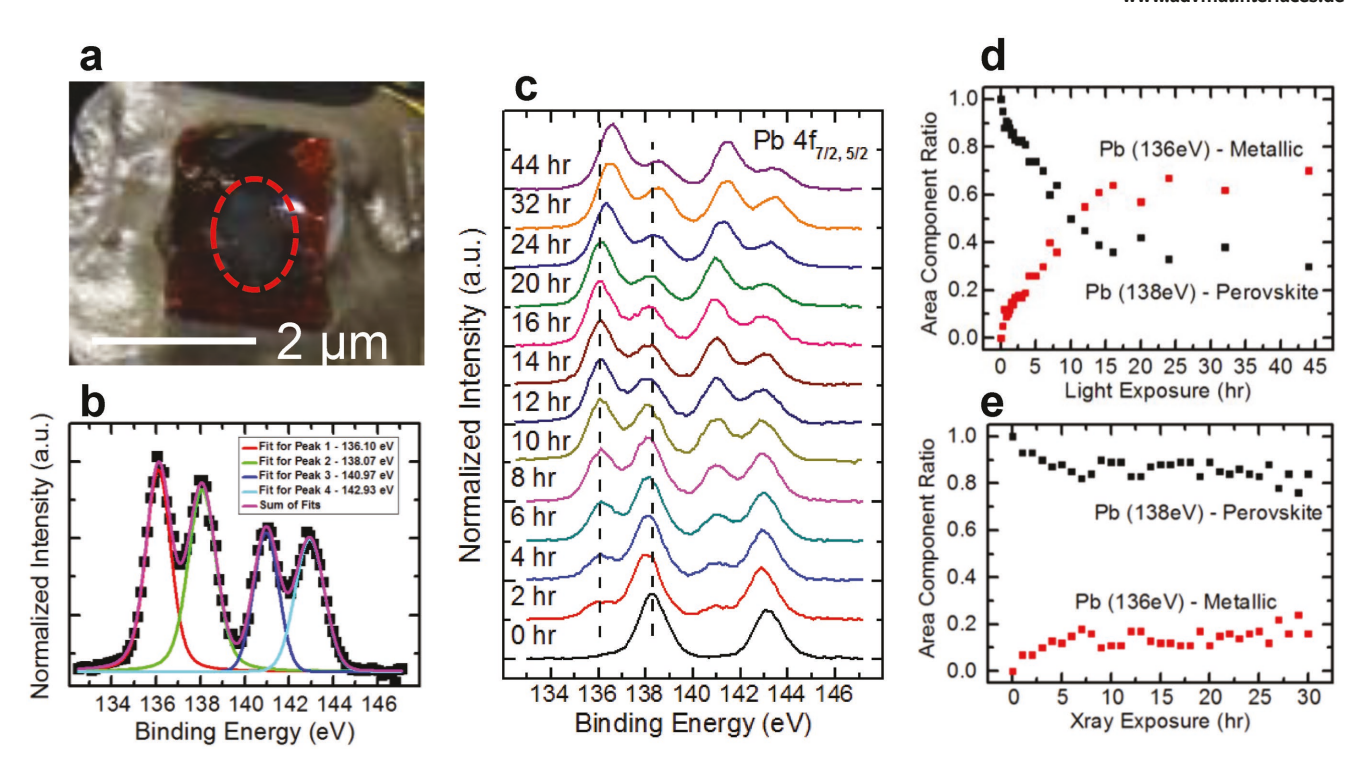


Figure 1. a) A photograph of a light exposed $CH_3NH_3PbBr_3$ single crystal, the red dashed circle represents the region exposed to the illumination. b) It shows how the spectra were fitted with four distinct Voigt profiles. c) A stack plot of the Pb $4f_{7/2}$ and $4f_{5/2}$ core levels with increasing light exposure. Each spectrum was normalized to one for perspective. d,e) The ratio of perovskite Pb to metallic Pb with increasing light exposure and X-ray exposure, respectively.

from a translucent orange to a dull and opaque metallic color and the transformed region was the same approximate size and position of the laser spot. Meanwhile, the surrounding regions appeared largely unchanged in appearance. The XPS analysis of the Pb 4f core levels is shown in **Figure 1**, and an image of a sample taken after the full exposure can additionally be seen in Figure 1a. For clarity, the silver around the orange crystal in the image is the conductive epoxy used for mounting and the red dashed circle highlights the illuminated position on the sample.

The most notable change in any of the core levels observed with XPS occurred in the lead spectra, and it can be seen in the Pb stacked plot shown in Figure 1c which specifically shows the Pb $4f_{7/2}$ and $4f_{5/2}$ spectrum with increasing light exposure. The initial perovskite Pb $4f_{7/2}$ and $4f_{5/2}$ core levels were located at 138.27 and 143.17 eV, respectively. After light exposure, a new component began to develop for each Pb core level ≈2 eV lower in binding energy (BE) from the perovskite species. The new and the original perovskite Pb components all shifted to a lower BE that occurred within the first hour of light exposure. The other perovskite core levels, including those of C, N, and Br, also had a similar initial downward BE shift and can be seen in Figure 2a. This initial shift was therefore considered a rigid one corresponding to the movement of the Fermi level within the bandgap. This type of movement indicates a p-doping of the perovskite, which may be attributed to the reduction of n-type traps on the surface from photogenerated charge carriers, or reversible photoinduced p-type trap formation.^[25]

After the initial BE shift, all of the spectral features (including C, N, and Br) began to gradually move to higher BEs and the new Pb features seemed to settle at around 136.6 and 141.4 eV for the $4f_{7/2}$ and $4f_{5/2}$ core levels, respectively. The new component represents a new chemical species and can be attributed to the formation of metallic lead, which has previously been documented at 137.0 eV for the Pb $4f_{7/2}$ core level.^[18,26,27] The small deviation in binding energy compared to the reported value is likely due to the local environment of the metallic lead surrounded by incompletely degraded perovskite. Various reports in the literature have suggested that metallic lead is detrimental to device performance, and in particular it has been suggested to act as an exciton quencher and provide a nonradiative recombination pathway.[26] Furthermore, the overall shift to higher BEs seen by all of the spectral features after the initial downward shift in the first 2 h was indicative of an overall n-doping of the perovskite, specifically the initial pristine perovskite Pb4f_{7/2} shifted from 138.27 to 138.48 eV. Such n-doping has also previously been reported and was associated to the reduction of the halide and to excessive Pb as an electron dopant.^[19,28]

The new metallic Pb component continued to grow in intensity with increasing light exposure, and in fact, it overtook the perovskite component after $\approx \! 10$ h of exposure. An example fitting presented in Figure 1b shows how the four distinct peaks were fit by Voigt lineshapes. For additional information regarding the secondary electron background subtraction and fitting routines, please see the Experimental Section. Using the fits of the strongest spectral response for our X-ray source,

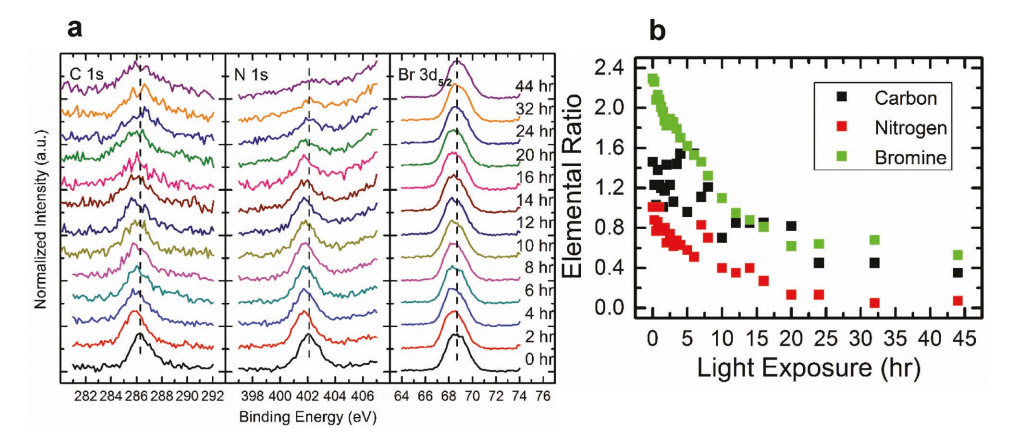


Figure 2. a) A stack plot of the C 1s, N 1s, Br $3d_{5/2}$ core levels with increasing light exposure. Each spectrum was normalized to one for perspective. b) It shows how the elemental ratio of the surface changes for C, N, and Br. The ratio is calculated by normalizing each element's signal to the lead overall intensity.

which for lead occurs in the $4f_{7/2}$ core level, the ratios between the perovskite component (≈ 138 eV) and the metallic component (≈ 136 eV) were computed. This ratio is plotted in Figure 1d, and it shows how this ratio changed over the entire exposure. By the end of the 44 h of light exposure, the metallic lead component made up $\approx 70\%$ of the overall lead signal and the remaining 30% signal came from the perovskite component. It is possible that saturation had not been reached by the end of 44 h of light exposure, and additional exposure may have continued the conversion of the perovskite Pb into metallic Pb.

For full transparency, we have previously observed^[7] this new metallic Pb also being created by the probing X-ray used during XPS in other studies on these single crystals and we wanted to ensure that the degradation in this report was mostly occurring from the light and not the measurement conditions. Therefore a separate measurement study was also performed where the sample was continuously exposed to the probing X-ray. The comparison study's ratios of the metallic and lead component created by the X-ray can be seen in Figure 1e, and here, the metallic lead appeared to stay less than ≈20% of the overall Pb signal. We also looked at the effects of leaving the sample in the vacuum for an extended period of time, as there have been some reports of vacuum induced degradation.^[29,30] Very little metallic lead was observed in the pure vacuum exposure study and what little was seen could be attributed to the probing X-ray, though perhaps longer vacuum exposures would have produced more similar results to the previous reports. Significantly less metallic lead was produced in the vacuum and X-ray exposure studies than the light illumination study, despite experiencing substantially more X-rays or prolonged vacuum exposure. This strongly suggests that the majority of metallic lead observed was indeed a result of light illumination and not the measurement conditions. More information and details regarding the X-ray and vacuum exposure studies can be seen in the Supporting Information, and the Pb stack plots can be seen in Figures S4 and S5 of the Supporting Information.

Again, the other perovskite elements' core levels, C1s, N1s, and Br $3d_{5/2}$, whose plot stacks are shown in Figure 2a, also saw similar binding energy shifts as was seen in the Pb $4f_{7/2, 5/2}$ features. Though, these elements did not appear to develop

any new components as previously described for Pb, and this indicated that they did not change their chemical state. Furthermore, their overall signal rapidly decreased in intensity in comparison to the Pb signal and their core levels substantially broadened with increasing light exposure. The surface's atomic ratios were calculated by taking these core levels fitted peak areas and normalizing them to the total Pb area (metallic plus perovskite) and their atomic sensitivity factors. A plot of these calculated ratios for C, N, and Br throughout the light exposure measurement is displayed in Figure 2a, and as shown in the plot, the surface saw significant losses in C, N, and Br concentrations. At ≈10 h of light exposure, 50% of the perovskite appears to have been degraded as about 50% of the C, N, and Br were lost and about 50% of the perovskite Pb was converted into metallic Pb. Interestingly, these ratios did not tend straight toward zero and in particular, the Br concentration seemed to level out at around 15 h of exposure. Our initial interpretation was again there was some sort of diffusion limited degradation process going on, as we have previously reported in the light induced degradation of CH₂NH₃PbI₃ coevaporated thin films.[18]

We suspected that the perovskite surface was decomposing into CH3NH3Br and PbBr2, before the PbBr2 further decomposed into metallic Pb and Br2. The elements C, N, and Br, could then simply leave the surface during the light exposures as degraded volatile components similar to simple outgassing. In fact, we actually observed the main chamber's ion gauge have small pressure increases on the order of 10⁻¹¹ Torr during the light exposures. In a follow up measurement, a residual gas analyzer (RGA) was able to record the small pressure increase which corresponded with the light being turned on and off repeatedly every 60 s which can be seen in Figure S6c of the Supporting Information. But unfortunately, the RGA was unable to conclusively determine which molecules were leaving the surface. Again though, the loss in surface concentrations and the core level shift to a higher binding energy are consistent with the previous report that showed that HOIPs have compositional dependent self-doping.[28] The previous report observed self-doping in CH3NH3PbI3 thin films by changing the ratio of the two precursors, methylammonium iodide (MAI)

and lead iodide (PbI2). Here though, the loss of the C, N, and Br induced by light exposure left behind a lead rich surface that saw a strong n-type shift compared to the initial chemical state of the freshly cleaved perovskite.

As a small caveat, one of our initial concern about the measurement was that the sample might have actually been degrading from heating due to the light illumination rather than the light exposure, as an early report suggested that perovskite had an extremely low thermal conductivity.^[8] More recent reports however have suggested that perovskite is a bit more conductive than initially reported.[9,31] A model based upon Abbott's heating calculation[32] was used to estimate the approximate heating due to the CW laser using various parameters reported in literature for HOIPs. The sample was sitting upon a stage which acted as a large thermal reservoir, and the estimated temperature increase ranged from ≈1 K as the best case to ≈15 K as the worst case. Thus, while we do not believe the observed changes were due to heating degradation, the small temperature increase may have enhanced ion diffusivity. This calculation is briefly discussed in the Supporting Information.

3. SEM/TEM Results

After finishing the XPS measurements, the sample was rapidly transferred into the SEM system in order to record the surface's morphological changes due to the light exposure, and the SEM images are shown below in **Figure 3**. In comparison to a freshly cleaved surface shown in Figure 3a which appeared smooth and almost terraced, the light exposed region's surface in Figure 3b was substantially transformed and roughened. Large globular clusters made up a majority of the surface, and we believe these clusters were the left behind metallic lead coalescing together since the metallic lead made up the predominate amount of the remaining XPS signal at the end of the exposure. Another spot

on the sample that was far away from the light exposed region is shown in Figure 3c. The region also appeared roughened in comparison to the freshly cleaved surface, but its surface features were substantially smaller and more uniform than the light exposed region.

On a serendipitous whim, microscopic trenches were created by an FIB in an attempt to investigate the change in the surface's appearance from the translucent orange to the dull opaque metallic color. Unexpectedly, large pockets of empty space ≈1-3 µm down into the material were observed in the exposed region and they are shown in Figure 3e. These voids were also seen in several other FIB trenches created in the light exposed region, and this ensured that they were not just some kind of one-off, shown in Figure S7 of the Supporting Information. They were completely surprising to us, as they were occurring far too deep into the material for XPS or any of our other standard techniques to give any kind of indication of their existence. The voids were also strikingly absent from the FIB milled trenches recorded for the freshly cleaved surface seen in Figure 3d and the other region that was not exposed to light shown in Figure 3f. These images serve as direct evidence that these voids were not created by the FIB milling process or due to prolonged vacuum exposure, but rather as a direct result of the light illumination. They also suggest that some process far more complicated than simple outgassing must be going on, or these empty pockets would have otherwise been expected at the surface. Furthermore, the beam damage due to the dosage behaved differently in the light exposed region as cracks that formed did not propagate across the void layer. While in the other regions, damage cracks appeared to propagate straight down into the material. While this observation was quite qualitative, the difference in behavior was indicative that this void layer was acting as some kind of boundary layer, and the difference in behavior was likely due to variations in the thermal or electrical properties between the upper and lower regions. Some more images and brief discussion about the

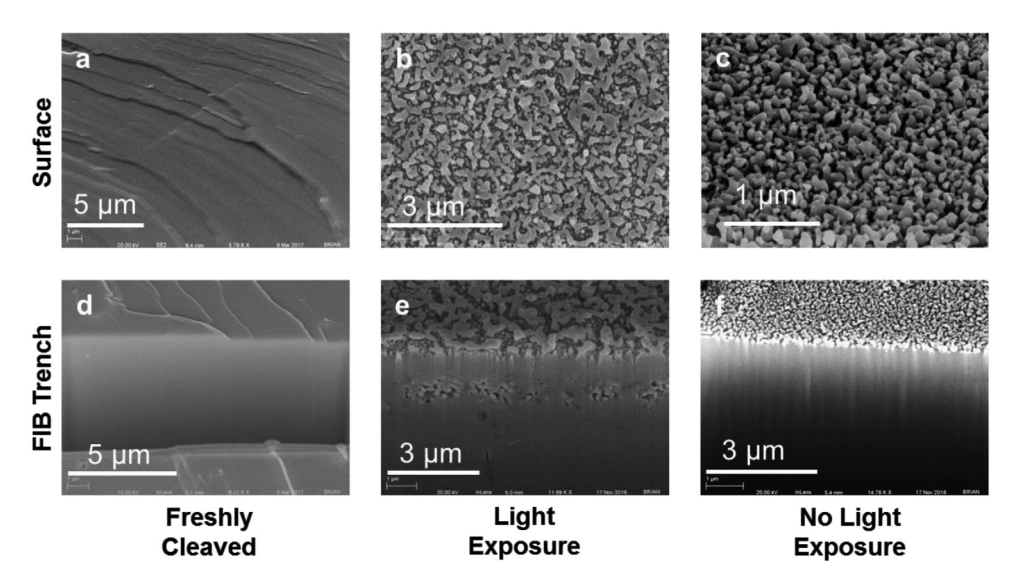


Figure 3. a–c) The SEM image of the surface of a freshly cleaved, light exposed, and no light but vacuum exposed samples, respectively. d–f) The FIB milled trenches for the freshly cleaved, light exposed, and no light but vacuum exposed samples, respectively. The FIB milled trench of the light exposed region revealed voids about 1–3 μm deep into the material.

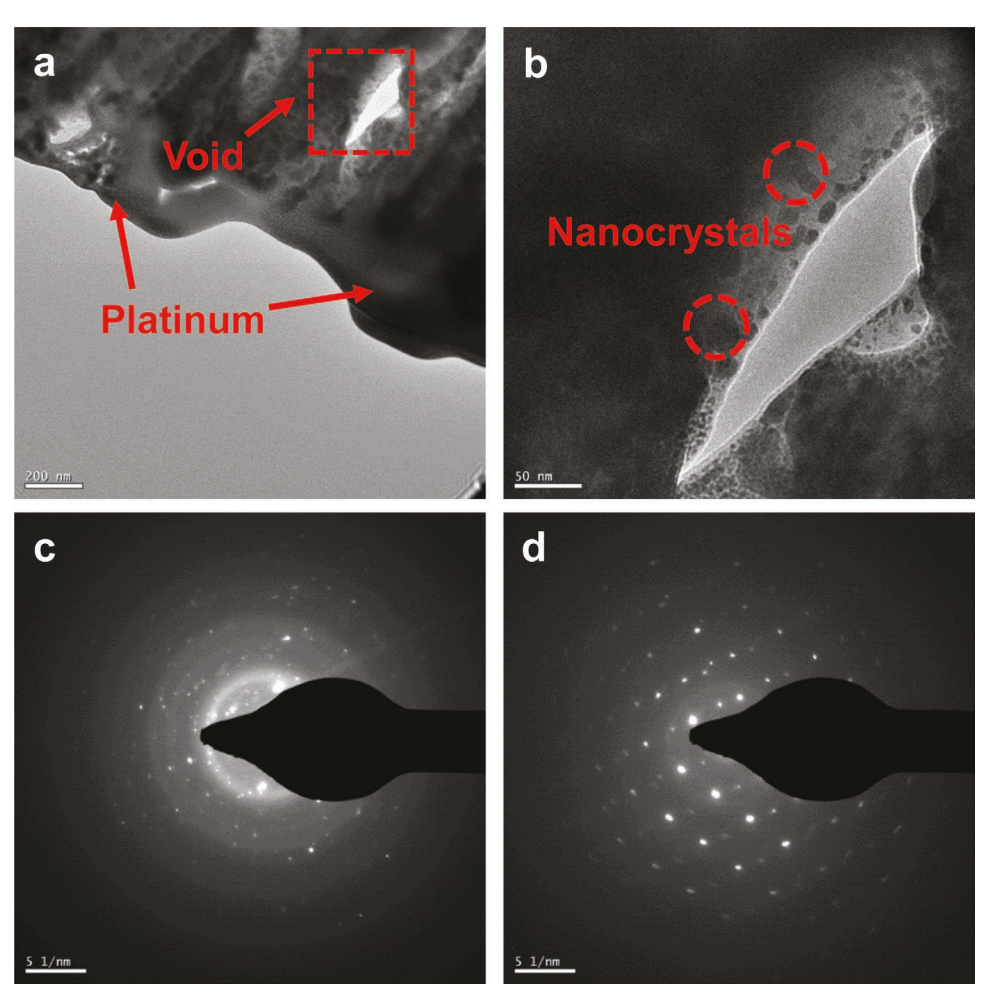


Figure 4. a) The TEM image of the top surface. The amorphous Pt layer used to protect the surface is visible and a red dashed box highlight a particular void shown in (b). c,d) The electron diffraction patterns from the top surface and the underlying bulk, respectively.

beam damage are further shown in Figure S8 of the Supporting Information.

In order to characterize more completely the chemical and morphological changes that were seen, an FIB liftout process was performed that removed a thin vertical slice, or lamella, of the exposed region which was then inserted into the TEM. The interaction volume is substantially smaller in the TEM compared to the SEM, and this facilitated a nanoscale resolution to view the regions above, below, and around the voids.[33,34] The FIB liftout process is briefly described in the Experimental Section, and it is documented in Figure S9 of the Supporting Information. After inserting into the TEM, quantitative energy dispersive X-ray spectroscopy (EDX) measurements were made on the lamella. The measured elemental ratio of Pb to Br near the surface was 1.00:1.40. This region was extremely deficient in Br for HOIP materials and was in good agreement with the XPS measurements for the surface. In the region far below the voids, which represents the underlying bulk, the ratio was 1.00:3.11 and is near the ideal ratio of 1:3. These measurements strongly suggest that the chemical changes were limited to the top surface and near the void layer. Qualitative EDX mapping were also performed, but offered no extra information. The

EDX mappings can be seen in Figure S10 of the Supporting Information.

Numerous other TEM images were collected after the EDX measurements and a select few are shown in Figure 4. The image in Figure 4a shows the top layer of the lamella, it shows one of the voids in the red dashed box and the amorphous Pt layer that was initially deposited to protect the surface during milling. A zoomed in view of the void in the box is shown in Figure 4b. Around the edge of the void, amorphous redeposition from the milling can be seen forming an interface with remaining degraded material. Perhaps more interestingly, there were also large black ovaloids around the voids that upon closer inspection showed lattice planes. FIB milling would not produce a crystalline structure as deposition and milling are largely random processes. This would suggest that the ovaloids were in the sample before milling and that they were actually nanocrystals. These nanocrystals appeared to be randomly oriented, as they did not all satisfy the Bragg condition in a single image (or single angle). So from these observations, it appeared that the single crystal was breaking apart in the upper region from the light exposure. Some additional higher magnification images are shown in Figures S11 and S12



www.advmatinterfaces.de

of the Supporting Information, and the lattice planes are more obvious.

To further confirm the change in crystallinity, electron diffraction patterns were collected from the regions near the degraded surface and deep in the bulk far below the voids, they are shown in Figure 4c,d, respectively. The diffraction pattern from the surface in Figure 4c is composed of large rings and some discrete spots, and this indicates that the region was predominately polycrystalline with a few regions of high crystallinity. This diffraction pattern is then in good agreement with the previous images that saw some randomly oriented nanocrystals. Whereas, the bulk diffraction pattern shown in Figure 4d, shows a highly repeating 2D pattern and indicates that sample's bulk had at least two dimensions of long range order. While the bulk's electron diffraction pattern was certainly not perfect, it closely resembled the expected pattern for a perovskite cubic structure from the [111] direction.^[35]

4. Void Formation Discussion

The substantial changes to the surface's appearance and crystallinity, as well as the creation of the void layer in the perovskite by light exposure, was an unexpected and intriguing result. Recently, Murali et al. have also observed the surface of CH3NH3PbBr3 single crystal restructuring into polycrystalline.[36] Additionally, while not directly mentioned in their main article, similar singular and sporadic voids can be readily distinguished from the cross-section SEM pictures in Murali's Supporting Information.[36] They however attributed this restructuring to the incorporation of H₂O into the structure, and this cannot explain the restructuring seen here as our light exposures and measurements occurred in a UHV chamber. While these voids were initially quite baffling, they strongly resembled the Kirkendall voids seen in literature which are sometimes also referred to as pores.[37] These Kirkendall voids sometime form as a byproduct of the more general Kirkendall effect which is associated with binary interdiffusion, or more bluntly, the intermixing of two distinct materials. Briefly, the effect is the motion of the boundary layer between the two materials arising from differing intrinsic diffusion rates across the interface, and has historically been examined in binary metal or alloy systems.[38] Interestingly, the initial work by Smigelskas and Kirkendall in the 1940s provided early experimental evidence for interstitial and vacancy mediated diffusion, where the diffusing species may have varying diffusion coefficients, which was fundamental to understanding the overall Kirkendall effect. Both interstitial and vacancy mediated diffusion has been well documented in other materials with the perovskite structure and their transport mechanisms are still widely being studied due to their influence on the materials properties.^[39] Now given enough time for the sufficient intermixing between the two materials, the differing diffusion rates will create a densification on the side with the slower diffusion and an increasing number of vacancies on the side with the faster diffusion. At high enough concentrations, these vacancies can begin to aggregate and accumulate into voids around the boundary layer.^[40] The void formation and the Kirkendall effect are still being investigated today,[41] as they can induce stress and deformations on the macroscopic scale. In the extreme case where the voids continue to aggregate and grow, the previously two distinct layers can fully delaminate from one another. Recently, some researchers have actually started using the Kirkendall effect to fabricate nanoscale structures.^[42,43]

To the best of the author's knowledge, no Kirkendall effect or effect similar to it has been discussed or documented in the literature concerning the HOIP materials. As such, no Kirkendall effect or voids were initially expected, nor was it immediately apparent on how a similar effect could even apply to this study. In fact, it cannot be the Kirkendall effect in the traditional sense as there is only one material initially and no boundary region. In this investigation, we observed a decrease in the XPS intensity from the C, N, and Br core levels and a pressure increase during the light exposures, which both strongly suggested that the perovskite was decomposing under illumination in the vacuum system. The volatile components were simply boiling off in the UHV chamber due to an exceptionally large mean free path, while the HOIPs lead remained behind as metallic lead from the decomposition. These observations did not directly pinpoint which specific species were playing a part in the diffusion effect, but we can infer that they involved the elements C, N, and Br. Perhaps they were diffusing as CH₃NH₃⁺ or Br⁻ ions, where upon reaching the surface, they react to form some volatile compound and leave. Now, one possibility to tie in something akin to the Kirkendall effect, is that as the volatile components continued to leave the surface, a chemical gradient began to build up. In this scenario, it is not that there is necessarily two competing intrinsic diffusion coefficients, but rather a net flux of precursors to the volatile components from the bulk to the surface with vacancies moving in the opposite direction. This makes some sense, as the diffusion flux is proportional to the gradient of the chemical potential which for simple dilute systems is then proportional to the chemical concentration gradient. Another possibility is that the diffusivity of the diffusing species depended upon the light illumination. The light penetration depth at 408 nm was expected to be on the order of 0.1 μ m, [44] which is close to the depth, 1–3 μ m, that the void layer formed at. Then, the top illuminated layer had a higher diffusivity than the underlying region where the light had been substantially attenuated, which resulted in the differing diffusion rate which is similar to the more traditional Kirkendall effect in a binary system. While both of these ideas are plausible, it is important to point out that the traditional Kirkendall effect and the observations made in this study must purely be a result of diffusion. These ideas and the observations in this study certainly begin to make sense in respect to the broader discussion of ionic migration in HOIPs, as will be discussed briefly, however, there was no external potential or bias to drive ion migration and the samples were well grounded in this study. This implies that the chemical variations and voids seen here, must be a result of the light illumination and some kind of diffusion process, which is in striking contrast to other studies that saw similar chemical degradation due to ion migration.

As previously mentioned, recent reports concerning ion migration in HOIPs begin to put the observations in this study onto a more solid footing. These reports should be considered relevant to diffusion discussions, as ion migration and diffusion





www.advmatinterfaces.de

are fundamentally related via the ion's mobility. Gottesman's initially proposed that under working conditions CH₃NH₃PbI₃ films underwent a lattice softening as the methylammonium ions had an enhanced rotational freedom,[45] and then later Zhou reported a giant photostriction effect in CH3NH3PbI3 single crystals due to a weakened binding between the methylammonium ion and the lead iodide framework.[46] It is reasonable to expect a similar effect on the CH₃NH₃PbBr₃ single crystals used in this study, and the strain created under illumination would cause the surface to break apart from single to polycrystalline as observed. The small heating effect suggested by the heating model in the supplementary material, may also imply a small amount of thermal expansion. It is difficult however to compare the photostriction to any potential thermal expansion as it is still under active investigation. These newly created grain boundaries will importantly act as channels that facilitate faster ion migration or diffusion and this has also previously been reported by Huang's group, where ultrafast ion migration was observed in CH3NH3PbI3 polycrystalline thin films and suppression in single crystals. [47,48] They then further suggested lower activation energies for ion migration under illumination, and this would imply that the illuminated region would indeed have a larger diffusion coefficient than the region below the light's penetration depth. Additionally, these new grain boundaries, as well as the surface, could act as sources and channels for vacancies which were necessary for the void formation in the Kirkendall effect. While these proposed ideas seem plausible, further investigation will be required to precisely determine the underlying mechanism(s).

5. Conclusion

The material and structural degradation that was observed during these measurements would be extremely detrimental to a PSC device's performance, and yet, there have been numerous long term operational studies where devices have lasted hundreds to thousands of hours under continuous illumination.[49,50] The fairly obvious question is if light illumination is indeed so harmful, why have no similar observations been made before? One such criticism may argue that this diffusion process only occurred as a result of being left in the UHV chamber where the volatile components readily boiled off, while in a real device these volatile components would be trapped inside the device between the adjacent layers. However as previously mentioned, Murali's recent report[36] showed similar voids, where their sample was left in ambient and presumably atmospheric conditions, suggesting that the void formation does not require vacuum conditions to occur. We additionally did not observe voids in regions that were left in the vacuum that were not exposed to the light, indicating the light played a pivotal role in the formation of our voids.^[51] It may also be difficult or impossible to ever observe similar void formation as seen in this study in any real HOIP devices, as a device's active perovskite layer is on the order of 300 nm and the void formation in these single crystals occurred over the range of several micrometers. If the voids ever did form in a real device, they would likely significantly alter the mechanical, thermal, and electrical properties of the layer and may deteriorate device

performance. However when considering a real device, the lack of voids in a perovskite layer does not necessary signify that a similar diffusion process to the one seen here was not occurring, as the void formation appears to require an appreciable concentration of vacancies before they begin to nucleate and aggregate. This effect may be especially important when considering nanoscale HOIP devices such as nanoemitters, as the Kirkendall effect has previously been used to create nanowires and hollow nanoparticles, [42,43] which may be beneficial or detrimental depending on the desired application.

Therefore, our chief concern from these observations is not whether similar void formation is occurring in a real device. Rather, it is that if such a degradation is occurring in real devices under illumination, that the diffusing components produced in the HOIP layer or the other device layers are actively diffusing into one another, creating an irreversible and ultimately detrimental chemical reaction as others have reported previously. [52-54] If this is the case, there may be more of a need for diffusion barrier engineering, to prevent such reactions from occurring.^[55] In diurnal illumination cycling of HOIP devices, substantially accelerated device degradation was seen in comparison to prolonged continuous illumination exposures.^[51] This unique "fatigue" effect in HOIP solar cells may be related to a similar diffusion or ion migration effect as seen in our light stability study, and suggests further research into these phenomena in devices.

These combined measurements showed that light illumination induced chemical and structural degradation in the CH₃NH₃PbBr₃ single crystals while in UHV conditions. The XPS measurements were able to monitor the chemical decomposition with increasing light exposures, and they showed that the C, N, and Br elemental components were decreasing on the surface and that the Pb component was being converted from perovskite to metallic Pb. Follow up measurements were able to show small pressure increases, and suggested that the C, N, and Br elemental components were leaving the surface as degraded volatile components which were perhaps in the form of MABr or Br₂. SEM images of the surface and of FIB trenches were collected, and the images showed distinctive voids formed in the region that was exposed to illumination while in the UHV. Additional TEM measurements performed on an FIB liftout lamella further confirmed the chemical and structural degradation seen before. EDX measurements showed how the surface was significantly deficient in Br concentrations, while the bulk of the crystal far below the void formation had a nearly 1:3 Pb to Br ratio. TEM images and electron diffraction patterns showed that the single crystal was breaking apart into nanocrystals under illumination. A model based of the Kirkendall effect and relevant HOIP diffusion ideas was put forward, and it was ultimately discussed in context to the long term stability of PSC devices under illumination. As the reader is well aware, this study is not a real device under working conditions, real devices and the perovskite layer are currently considered to be much more stable than observed in this study. The UHV conditions used during illumination may have allowed the volatile components induced by the illumination to readily leave the surface, but the pure vacuum conditions alone without illumination did not see such degradation. Overall, substantially more research needs to be performed on the stability of the HOIP layers in



www.advmatinterfaces.de

actual devices under illumination, with a particular interest of components diffusing or migrating into or out of the active perovskite laver.

6. Experimental Section

Sample Growth, XRD Characterizations: The growth of the CH₃NH₃PbBr₃ single crystals used in this study have previously been described in ref. [20]. Briefly though, in a 20 mL vial 0.64 M of lead bromide (PbBr $_2$) and 0.8 M of methylamine bromide (MABr) were dissolved in a 5 mL N, N-dimethylformamide solution. Foil was then used to seal the vial, a tiny hole was made in the seal, and then the vial was placed in a dichloromethane (DCM) environment. The tiny hole was made in order to allow DCM to slowly enter and permeate the solution to act as an antisolvent, and the single crystals slowly grew over 2 days. Powder XRD measurements of the crystals were previously made and were also described in ref.[20] Additional textured XRD measurements were performed to confirm the orientation of the crystals and their cleave plane used during the photoemission measurements. The new XRD measurements were made with a Phillips X'pert MPD located at the University of Rochester, where the X-rays were produced from a Cu anode using a 40 kV and 30 mA generator setting.

Sample Mounting: In order to obtain a pristine surface which are necessary for reliable photoemission spectroscopy studies, the samples were mounted in such a way that the top surface of the crystal could be cleaved off in situ. The crystals were first placed in a conductive UHV epoxy (Epoxy Technology, Product EJ2189-LV) on top of conductive Au-coated silicon substrate, and it was allowed to cure at room temperature and atmosphere for 24 h. The conductive epoxy was necessary as it allowed the sample to be properly ground during the photoemission measurements. The following day, a small amount of another UHV epoxy (Varian Vacuum Technologies, Product Torr Seal) was used to cover the top surface of the crystal in such a way that the two epoxies had no direct contact. A small tungsten rod was placed in the wet top epoxy so that when cured, the tungsten rod could be gently pressed into a gate valve once inside the vacuum system. When the tungsten rod was then broken off, the attached cured epoxy and the top surface of the crystal were additionally cleaved off.

UHV Chamber and Light Exposure: The UHV system used during this study was located at the University of Rochester and consisted of two interconnecting chambers, a transfer chamber used for cleaving and an analysis chamber used for the XPS measurements. When the transfer chamber was sufficiently pumped down, the surface of the crystal was cleaved off by pushing the tungsten rod into a gate valve. The samples were cleaved in the transfer chamber with a base pressure of 10^{-6} Torr before rapidly being transferred to the analytic chamber with a base pressure of 8×10^{-11} Torr. Once transferred and aligned, the sample maintained a fixed position for the entirety of the XPS measurements and light exposures. A small diode laser was attached to a viewing port on the analytic chamber, and its beam position could be monitored with a microscope attached on top of the analytic chamber. The laser's spot size formed an ellipse on the sample surface, whose semimajor and semiminor axes were 1.65 and 0.66 mm, and its power was also measured to be 42 mW. The intensity was fairly uniform over the entire spot, and had an average intensity of 7.21 mW mm⁻². This is approximately seven times the strength of the solar intensity (1000 W $m^{-2} = 1.0$ mW mm^{-2}). The diode laser's wavelength was 408 ± 5 nm. The timed exposures and following measurements occurred contiguously for ≈3 days. The measurement spot received a full light exposure amount of 44 h, and at no point was the light illumination source and probing X-ray source on at the same time.

XPS: The surface's elemental composition was determined from high resolution XPS measurements. The monochromatic Al K α X-rays (1486.6 eV) used for the measurements were initially produced by an X-ray gun with an Al anode running at 10 kV and 20 mA. The produced X-rays were then passed through a temperature regulated quartz crystal,

and the diffracted X-rays that hit the sample were monochromatic and formed a spot size ≈ 1 mm in diameter. The spectra for the C1s, N1s, Br3ds/2, and Pb4f7/2 core levels were collected after each timed light exposure, and they were fitted with a Voigt profile after removing a Shirley-type background correction. The ratios of the Lorentzian and Gaussian component were not fixed during the peak fitting routine. Lastly, the elemental ratio of the surface was calculated taking the element's core level signal intensity (fitted area) and dividing it by their atomic sensitivity factor and the normalized lead intensity. This set the overall lead signal to one. Lead was chosen as the reference because it was not expected to form a volatile compound that could readily leave the surface.

SEM: The SEM imaging, FIB milling, and subsequent liftout process were performed in the Zeiss Auriga SEM instrument located at the University of Rochester's URnano center. For the imaging, the SEM typically had an accelerating voltage around 20 kV and a working distance between 5 and 10 mm. The accelerating voltage, beam current, and the final beam aperture were reduced whenever possible to minimize beam damage. Beam damage would appear rapidly under high beam dosages and presented itself in the formation of large cracks in the surface. Images were often collected after focusing upon one area, before rapidly moving and collecting in a nearby undamaged region.

FIB Milling and Liftout: An accelerated focused gallium ion beam produced from a liquid metal source was used to ablate material away by knocking out atoms and molecules, and it created the trenches for imaging and was used for the subsequent lamella liftout process. Before any milling could occur, the sample's surface was precisely positioned at the eucentric point where the focus of the SEMs electron beam was coincident with the focused ion beam position. The gallium ions were accelerated at 30 kV with a beam current that typically ranged from 120 pA to 4 nA depending on the milling size and speed. At these conditions, no ion beam damage was evident and any damage only seemed noticeable after imaging with the electron beam. The FIB milled trenches were created by two milling steps. The first step was a rough mill that was created by scanning the FIB over an isosceles trapezoid, which ablated material away to leave behind a trench 10-20 μm deep and wide. A second follow up milling, which was much smaller and precise, was done just on over the milled wall. This smoothed up the surface and removed some of the milling artifacts from the initial milling.

To protect the top surface of the lamella from redeposition of the ablated material during the liftout process, a thin layer of Pt was initially deposited on the top surface and was ≈100 nm thick. The Pt was dissociated from a Pt organic gas by the ion beam before then falling on the sample. The initial lamella before refinement was $\approx 3~\mu m$ thick, 15 µm wide, and 10 µm deep, and was formed by first milling out trenches from the front, back, and left side. The stage was then further tilted and the lamella was then milled out from below, leaving the lamella only attached to the sample from the right side. A needle probe was drawn near the top left edge and was welded to the lamella with further Pt deposition. The remaining connection on the right side was then milled away, leaving the lamella now disconnected from the sample's surface. The lamella was then carefully moved away from the sample and toward a TEM grid, where it was then welded again with Pt deposition. After being attached to the grid, the needle and a small portion of the lamella were cut off with the focused ion beam. Lastly, further refinement milling were performed on the front and back of the lamella to reach the desired thickness, which was ≈100 nm thick. This point was fairly evident as portions of the lamella began to appear transparent to the electron beam in the SEM. This process is fully documented pictorially in the Supporting Information.

TEM: The TEM bright field imaging, energy dispersive X-ray spectrometry, and electron diffraction patterns were collected on an FEI Tecnai F20 G2 Scanning transmission electron microscope located again at the University of Rochester's Urnano center. For the data collected, the TEM instrument typically had a beam with an accelerating voltage of 200 kV and had ≈0.14 nm resolution in TEM mode. The TEM additionally had a bottom mounted Gatan camera, which facilitated digital image captures. The EDX system was mounted near the sample

ADVANCED MATERIALS INTERFACES

and could collect X-rays produced from the beams interaction with the sample to produce a quantitative chemical analysis and high resolution chemical mappings.

Supporting Information

Supporting Information is available from the Wiley Online Library or from the author.

Acknowledgements

Y.G. initially conceived the project and continued to supervise throughout conception. H.W. and J.H. synthesized the CH₃NH₃PbBr₃ single crystals. B.E., C.W., and Y.G. carried out the XPS measurements. B.E. performed the SEM/FIB/TEM work. B.E. and Y.G. carried out the analysis. Y.G., J.H., and Y.Y. provided critical insights and discussions that led to ultimate interpretation of the results. B.E. and Y.G. wrote the manuscript, and all authors reviewed it. The authors declare no competing financial interests.

This work was supported in part by NSFCBET-1437656. J.H. acknowledges supports from AFOSRA9550-16-1-0299, NSFDMR-1420645, and NSFOIA-1538893.

The authors would like to acknowledge and thank Christine Pratt and Steven Burns for their assistance and technical knowledge with the X-ray diffraction measurements. The authors would also like to acknowledge and thank Brian McIntyre and Ralph Wiegandt for their technical assistance, knowledge, and invaluable discussions regarding the SEM, FIB, and TEM work and images.

Conflict of Interest

The authors declare no conflict of interest.

Keywords

Kirkendall effect, light stability, perovskites, solar cell, surface analysis

Received: August 6, 2018 Revised: August 31, 2018 Published online: October 8, 2018

- [1] A. Kojima, K. Teshima, Y. Shirai, T. Miyasaka, J. Am. Chem. Soc. 2009, 131, 6050.
- [2] NREL, Best Research-Cell Efficiencies, https://www.nrel.gov/pv/ assets/images/efficiency-chart.png (accessed: August 2018).
- [3] A. Babayigit, A. Ethirajan, M. Muller, B. Conings, Nat. Mater. 2016, 15, 247.
- [4] H. J. Snaith, A. Abate, J. M. Ball, G. E. Eperon, T. Leijtens, N. K. Noel, S. D. Stranks, J. T. Wang, K. Wojciechowski, W. Zhang, J. Phys. Chem. Lett. 2014, 5, 1511.
- [5] Y. Yuan, J. Huang, Acc. Chem. Res. 2016, 49, 286.
- [6] Y. Li, X. Xu, C. Wang, C. Wang, F. Xie, J. Yang, Y. Gao, J. Phys. Chem. C 2015, 119, 23996.
- [7] C. Wang, B. R. Ecker, H. Wei, J. Huang, Y. Gao, J. Phys. Chem. C 2018, 122, 3513.
- [8] A. Pisoni, J. Jacimovic, O. S. Barisic, M. Spina, R. Gaal, L. Forro, E. Horvath, J. Phys. Chem. Lett. 2014, 5, 2488.
- [9] G. Divitini, S. Cacovich, F. Matteocci, L. Cinà, A. Di Carlo, C. Ducati, Nat. Photonics 2016, 1, 15012.

- [10] X. Cao, Y. Li, C. Li, F. Fang, Y. Yao, X. Cui, J. Wei, J. Phys. Chem. C 2016, 120, 22784.
- [11] Y. Deng, Z. Xiao, J. Huang, Adv. Energy Mater. 2015, 5, 1500721.
- [12] T. Leijtens, G. E. Eperon, S. Pathak, A. Abate, M. M. Lee, H. J. Snaith, *Nat. Commun.* 2013, 4, 2885.
- [13] G. Murugadoss, S. Tanaka, G. Mizuta, S. Kanaya, H. Nishino, T. Umeyama, H. Imahori, S. Ito, Jpn. J. Appl. Phys. 2015, 54, 08KF08
- [14] S. S. Shin, E. J. Yeom, W. S. Yang, S. Hur, M. G. Kim, J. Im, J. Seo, J. H. Noh, S. I. Seok, *Science* **2017**, *356*, 167.
- [15] D. Bryant, N. Aristidou, S. Pont, I. Sanchez-Molina, T. Chotchunangatchaval, S. Wheeler, J. R. Durrant, S. A. Haque, Energy Environ. Sci. 2016, 9, 1655.
- [16] H. Yuan, E. Debroye, K. Janssen, H. Naiki, C. Steuwe, G. Lu, M. Moris, E. Orgiu, I. H. Uji, F. De Schryver, P. Samori, J. Hofkens, M. Roeffaers, J. Phys. Chem. Lett. 2016, 7, 561.
- [17] A. Merdasa, M. Bag, Y. Tian, E. Källman, A. Dobrovolsky, I. G. Scheblykin, J. Phys. Chem. C 2016, 120, 10711.
- [18] Y. Li, X. Xu, C. Wang, B. Ecker, J. Yang, J. Huang, Y. Gao, J. Phys. Chem. C 2017, 121, 3904.
- [19] H. Xie, X. Liu, L. Lyu, D. Niu, Q. Wang, J. Huang, Y. Gao, J. Phys. Chem. C 2016, 120, 215.
- [20] R. P. Xu, Y. Li, T. Y. Jin, Y. Q. Liu, Q. Y. Bao, C. O'Carroll, J. X. Tang, ACS Appl. Mater. Interfaces 2018, 10, 6737.
- [21] H. R. Byun, D. Y. Park, H. M. Oh, G. Namkoong, M. S. Jeong, ACS Photonics 2017, 4, 2813.
- [22] S. J. Yoon, S. Draguta, J. S. Manser, O. Sharia, W. F. Schneider, M. Kuno, P. V. Kamat, ACS Energy Lett. 2016, 1, 290.
- [23] H. Wei, Y. Fang, P. Mulligan, W. Chuirazzi, H.-H. Fang, C. Wang, B. R. Ecker, Y. Gao, M. A. Loi, L. Cao, J. Huang, *Nat. Photonics* 2016, 10, 333.
- [24] C. Wang, B. R. Ecker, H. Wei, J. Huang, J. Q. Meng, Y. Gao, Phys. Chem. Chem. Phys. 2017, 19, 5361.
- [25] E. T. Hoke, D. J. Slotcavage, E. R. Dohner, A. R. Bowring, H. I. Karunadasa, M. D. McGehee, Chem. Sci. 2015, 6, 613.
- [26] G. Sadoughi, D. E. Starr, E. Handick, S. D. Stranks, M. Gorgoi, R. G. Wilks, M. Bar, H. J. Snaith, ACS Appl. Mater. Interfaces 2015, 7, 13440.
- [27] R. Lindblad, N. K. Jena, B. Philippe, J. Oscarsson, D. Bi, A. Lindblad, S. Mandal, B. Pal, D. D. Sarma, O. Karis, H. Siegbahn, E. M. J. Johansson, M. Odelius, H. Rensmo, J. Phys. Chem. C 2015, 119, 1818.
- [28] Q. Wang, Y. Shao, H. Xie, L. Lyu, X. Liu, Y. Gao, J. Huang, Appl. Phys. Lett. 2014, 105, 163508.
- [29] I. Deretzis, A. Alberti, G. Pellegrino, E. Smecca, F. Giannazzo, N. Sakai, T. Miyasaka, A. La Magna, Appl. Phys. Lett. 2015, 106, 131904
- [30] S. Wang, Y. Jiang, Emilio J. Juarez-Perez, L. K. Ono, Y. Qi, Nat. Photonics 2016, 2, 16195.
- [31] Q. Chen, C. Zhang, M. Zhu, S. Liu, M. E. Siemens, S. Gu, J. Zhu, J. Shen, X. Wu, C. Liao, J. Zhang, X. Wang, M. Xiao, Appl. Phys. Lett. 2016, 108, 081902.
- [32] D. Abbott, B. Davis, B. Gonzalez, A. Hernandez, K. Eshraghian, Solid-State Electron. 1998, 42, 809.
- [33] M. Sugiyama, J. Electron Microsc. 2004, 53, 527.
- [34] J. Mayer, L. A. Giannuzzi, T. Kamino, J. Michael, MRS Bull. 2007, 32, 400.
- [35] T. Oku, Crystal Structures of CH3NH3PbI3 and Related Perovskite Compounds Used for Solar Cells, in Solar Cells – New Approaches and Reviews, Intech Open, London 2015.
- [36] B. Murali, S. Dey, A. L. Abdelhady, W. Peng, E. Alarousu, A. R. Kirmani, N. Cho, S. P. Sarmah, M. R. Parida, M. I. Saidaminov, A. A. Zhumekenov, J. Sun, M. S. Alias, E. Yengel, B. S. Ooi, A. Amassian, O. M. Bakr, O. F. Mohammed, ACS Energy Lett. 2016, 1, 1119.



ADVANCED MATERIALS INTERFACES

www.advmatinterfaces.de

- [37] L. Yin, P. Borgesen, J. Mater. Res. 2011, 26, 455.
- [38] A. D. Smigelskas, E. O. Kirkendall, Tech. Publ. Am. Inst. Min. Metall. Eng. 1947, 171, 130.
- [39] B. P. Uberuaga, L. J. Vernon, Solid State Ionics 2013, 253, 18.
- [40] J. A. Brinkman, Acta Metall. 1955, 3, 140.
- [41] K. Weinberg, T. Bohme, IEEE Trans. Compon. Packag. Technol. 2009, 32, 684.
- [42] Y. Yu, J. Li, D. Geng, J. Wang, L. Zhang, T. L. Andrew, M. S. Arnold, X. Wang, ACS Nano 2015, 9, 564.
- [43] A. E. Paz y Puente, D. Erdeniz, J. L. Fife, D. C. Dunand, Acta Mater. 2016, 103, 534.
- [44] B. Wenger, P. K. Nayak, X. Wen, S. V. Kesava, N. K. Noel, H. J. Snaith, Nat. Commun. 2017, 8, 590.
- [45] R. Gottesman, E. Haltzi, L. Gouda, S. Tirosh, Y. Bouhadana, A. Zaban, E. Mosconi, F. De Angelis, J. Phys. Chem. Lett. 2014, 5, 2662.
- [46] Y. Zhou, L. You, S. Wang, Z. Ku, H. Fan, D. Schmidt, A. Rusydi, L. Chang, L. Wang, P. Ren, L. Chen, G. Yuan, L. Chen, J. Wang, *Nat. Commun.* 2016, 7, 11193.

- [47] Y. Shao, Y. Fang, T. Li, Q. Wang, Q. Dong, Y. Deng, Y. Yuan, H. Wei, M. Wang, A. Gruverman, J. Shield, J. Huang, Energy Environ. Sci. 2016, 9, 1752.
- [48] J. Xing, Q. Wang, Q. Dong, Y. Yuan, Y. Fang, J. Huang, Phys. Chem. Chem. Phys. 2016, 18, 30484.
- [49] G. Grancini, C. Roldan-Carmona, I. Zimmermann, E. Mosconi, X. Lee, D. Martineau, S. Narbey, F. Oswald, F. De Angelis, M. Graetzel, M. K. Nazeeruddin, *Nat. Commun.* 2017, 8, 15684.
- [50] C.-Y. Chang, W.-K. Huang, Y.-C. Chang, Chem. Mater. 2016, 28, 6305.
- [51] F. Huang, L. Jiang, A. R. Pascoe, Y. Yan, U. Bach, L. Spiccia, Y.-B. Cheng, *Nano Energy* **2016**, *27*, 509.
- [52] Y. Kato, L. K. Ono, M. V. Lee, S. Wang, S. R. Raga, Y. Qi, Adv. Mater. Interfaces 2015, 2, 1500195.
- [53] K. Domanski, J. P. Correa-Baena, N. Mine, M. K. Nazeeruddin, A. Abate, M. Saliba, W. Tress, A. Hagfeldt, M. Gratzel, ACS Nano 2016, 10, 6306.
- [54] X. Zhu, J. Lee, W. D. Lu, Adv. Mater. 2017, 29, 1700527.
- [55] E. Bi, H. Chen, F. Xie, Y. Wu, W. Chen, Y. Su, A. Islam, M. Gratzel, X. Yang, L. Han, *Nat. Commun.* 2017, 8, 15330.